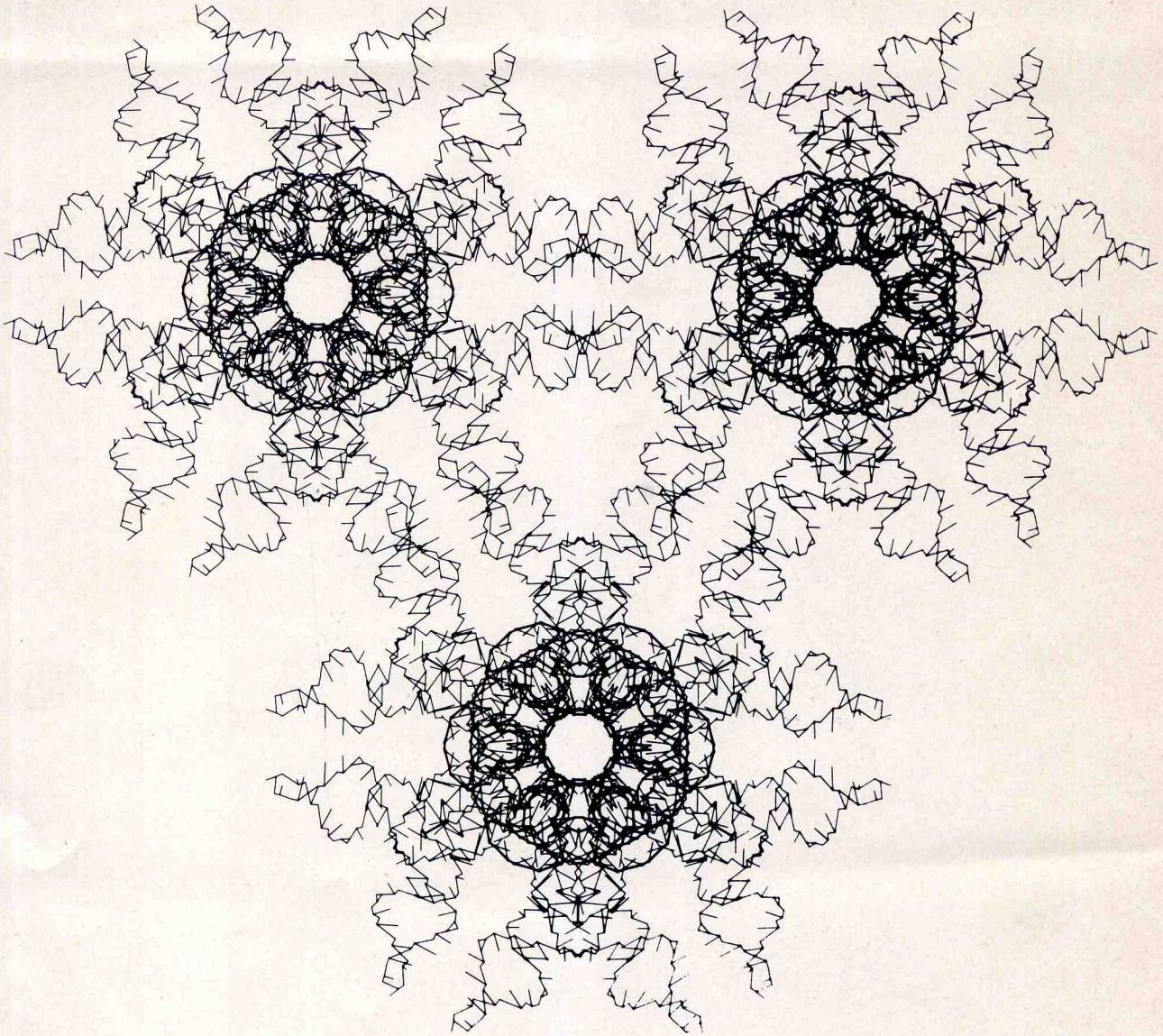


# nature

Vol 278 No 5700 8 March 1979 80p US \$2.25



**Crystal  
structure  
of eukaryotic tRNA**

## Crystal structure of a eukaryotic initiator tRNA

OUR understanding of the molecular structure-function relationship in tRNA rests mainly on three types of information. First, on the common sequence patterns which have emerged from careful examination of many primary structures<sup>1-3</sup>; second, a wide variety of spectral and other physical and chemical results must be accounted for by the molecular structure<sup>4-6</sup>; and third, there is the detailed image of the yeast tRNA<sup>Phe</sup> molecule independently determined and refined from two different—albeit similar—crystal forms<sup>7-10</sup>. It is also clear, however, that the molecular model deduced from the yeast tRNA<sup>Phe</sup> crystal structure cannot be easily reconciled with all structural requirements for function and is best considered a well-defined and stable canonical form of tRNA which is packed in an unusually well-ordered way in specific crystal lattices. Notwithstanding the enormous value of this canonical form in explaining the basic architectural features of tRNA, it is clearly important to image other crystalline tRNAs; particularly tRNAs that exhibit different functions (such as, initiators) or have significantly different covalent structures (for example, class III tRNAs)<sup>1</sup> or those that crystallise in different solvent conditions. We report here the initial results of the crystal structure determination of a eukaryotic initiator tRNA crystallised from a highly polar aqueous solvent<sup>11,12</sup>. Its architecture is essentially the same as crystalline yeast tRNA<sup>Phe</sup>, except for a small but significant difference in the position of the anticodon arm.

Our interpretation is based on a 4.5 Å electron density map prepared by the method of multiple isomorphous replacement (MIR) and augmented by direct methods<sup>13</sup>. The trace of the sugar-phosphate backbone is further constrained by four heavy-atom markers, each covalently linked to a specific residue and an elaborate network of crystallographic dyads upon which the

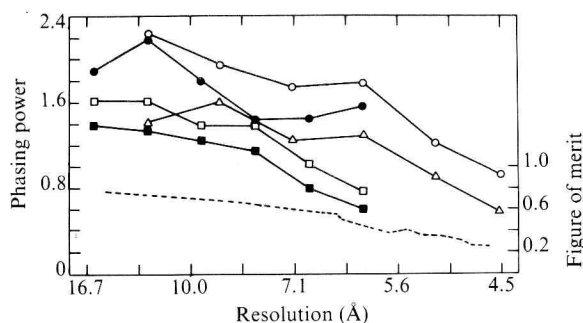


**Fig. 1** Phasing power  $(\sum |F_H|^2)^{1/2} / (\sum (|F_{PH}^{obs}| - |F_{PH}^{calc}|)^2)^{1/2}$  of five isomorphous derivatives plotted against resolution. They are gadolinium, lightly substituted, precession data (■); gadolinium, heavily substituted, precession data (□); gadolinium, oscillation data (△), pyridyl mercury acetate, precession data (●), and pyridyl mercury acetate, oscillation data (○). Figure of merit (---) is determined from MIR phasing<sup>33</sup> and has a mean value of 0.49 for all reflections to 4.5 Å resolution.  $F_H$  is the calculated heavy atom structure amplitude;  $(|F_{PH}^{obs}| - |F_{PH}^{calc}|)$  is the 'lack of closure' error between observed and calculated isomorphous derivative structure amplitudes.

molecule cannot intrude. The model presented here is based on a low resolution least-squares refinement procedure which assumes that the molecule is organised in four domains corresponding to the arms of the cloverleaf hydrogen-bonding pattern<sup>14</sup>.

The crystals have three important characteristics<sup>15</sup>. (1) They are grown from and stabilised in approximately 2M  $(NH_4)_2SO_4$  containing 5 mM  $Mg^{2+}$  and 2 mM spermine and no organic solvent. The 2M ammonium ion may alter the structural role attributed to  $Mg^{2+}$  and spermine in crystalline yeast tRNA<sup>Phe</sup> (refs 16-18). (2) Only 17.5% of the crystal volume is occupied

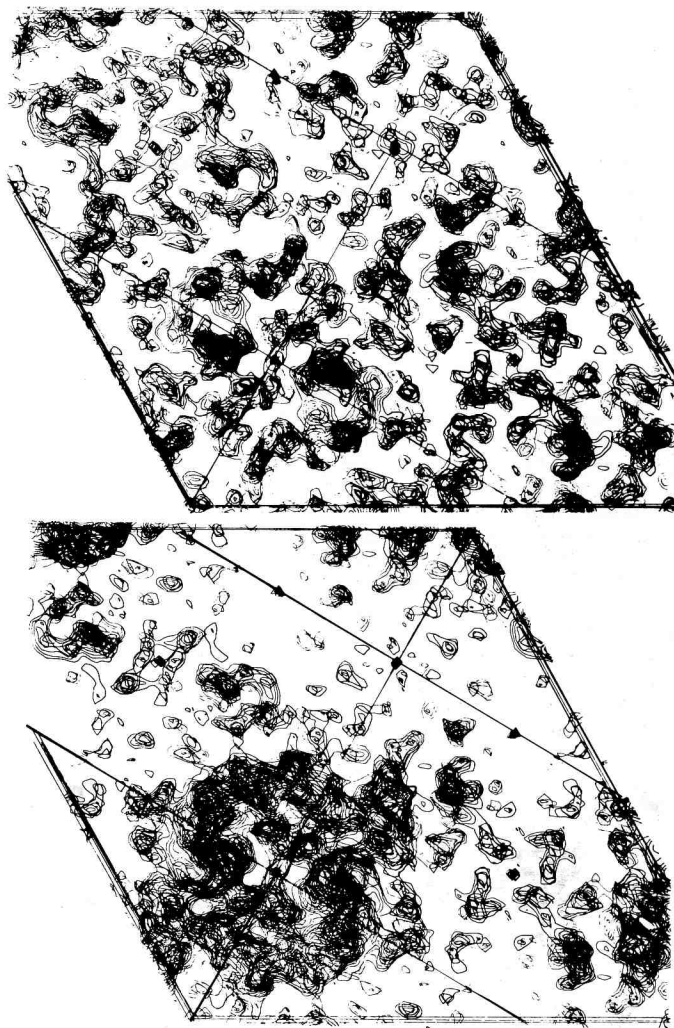


**Fig. 2** Comparison of 10 sections of the 4.5 Å map of yeast tRNA<sup>Met</sup> before (above) and after (below) the inclusion of 28 intense low resolution terms determined by matricial phase predictions. Both maps are contoured at the same intervals. Density cleared by this technique was ultimately shown to be noise, while density that was enhanced improved connectivity in the helical stems. Density on the dyad axes diminished.

by tRNA. Treating the remaining 82.5% as disordered solvent of uniform density was quite helpful in the structure analysis. (3) The crystal is poorly ordered, making accurate data collection very difficult and effectively impossible beyond 4 Å resolution. Data for the parent and three isomorphous heavy atom derivatives were collected initially to 6 Å by precession photography and extended to 4.0 Å by oscillation photographs in which a single crystal was devoted to each of ~30 overlapping 2.5° or 2° sectors. Figure 1 shows that there is useful phasing power in the best derivative to about 4.5 Å resolution. Schevitz *et al.*<sup>15</sup> presented a 6 Å analysis of the yeast tRNA<sup>Met</sup> crystal structure. Despite two heavy atom markers at iodine <sup>127</sup>I<sub>73</sub> (5-bonding onto cytosine at residue 73) and osmium <sup>192</sup>Os<sub>38</sub> the electron density could not be convincingly interpreted in terms of the molecular backbone. Even when the data for the parent structure and MIR phases were extended to 4.5 Å resolution and a third heavy atom marker at iodine <sup>127</sup>I<sub>8</sub> was used the map was still too 'noisy' to interpret confidently.

One particularly vexing deficiency in the MIR map was the inability to define the exact molecular boundary with confidence. As over 80% of the unit cell volume was solvent this structure was particularly amenable to phase improvement by solvent levelling if the molecular boundary could be accurately established<sup>19,20</sup>. The boundary was established by phasing the previously omitted very intense inner reflections ( $d > 14$  Å). In

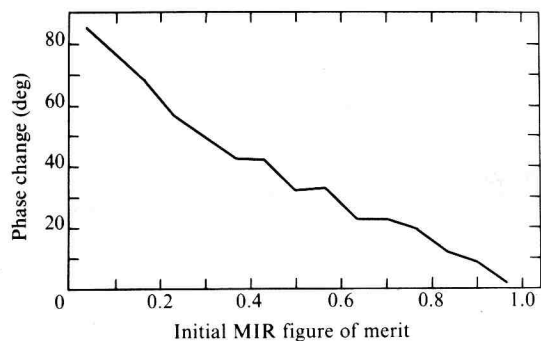


**Fig. 3** Final phase change in degrees resulting from direct methods (see text) as a function of the original figure of merit determined by conventional MIR phasing. Phase information from both sources was merged by multiplying together their respective phase probability curves after each cycle of combined solvent levelling and density modification. Note that those reflections predicted to have a high reliability by MIR phasing (figure of merit near 1.0) remained closely tethered to their MIR phase while those with a low MIR reliability (figure of merit near 0) tend to be more easily shifted toward phases calculated by direct methods.

the effort to secure high resolution data by extensively irradiating each crystal, these strong reflections were overexposed and far exceeded the dynamic range of even the most weakly exposed film. Even if relatively accurate amplitudes had been obtained for the parent and derivatives it is likely that the heavy

atom contribution would not have been strong enough to provide accurate difference amplitudes to phase the very strongest of these reflections. To circumvent this problem the inner core of intense parent intensities was accurately remeasured and the phases of 28 of the very strongest reflections were determined by applying matricial methods to the amplitudes and MIR phases of 107 known reflections. The technique is similar to that used by Podjarny *et al.* to extend the phases of triclinic lysome<sup>21</sup> and yeast tRNA<sup>Phe</sup> (ref. 22) to a higher resolution than the starting phase set. Here the procedure was used to extend phases to a lower resolution than the MIR phase set. The details of this work will be published elsewhere<sup>13</sup>; however, it is evident from Fig. 2 that there was substantial enhancement of the contrast between the molecule and the solvent. The improved map enabled us to confidently define 65% of the unit cell as solvent. New phases were calculated from a map in which the noise in the 'solvent' was levelled to a uniform average value and negative regions in the molecule attenuated<sup>23,24</sup>. These phases were merged with MIR phases and the 'density modification' procedure repeated for three cycles. Figure 3 shows that the phase improvement effected by density modification was most apparent for those reflections whose MIR phase was, in general, least accurate.

Four residues have been reacted stoichiometrically with covalently bonded heavy atoms. The heavy-atom markers were nicely distributed along the molecular backbone and provided a clear guide to the interpretation. (1) Iodine <sup>5</sup>C<sub>73</sub>: the third residue from the 3' terminus was labelled with iodine either by enzymatically rebuilding the 3' terminus with iodine <sup>5</sup>CTP and

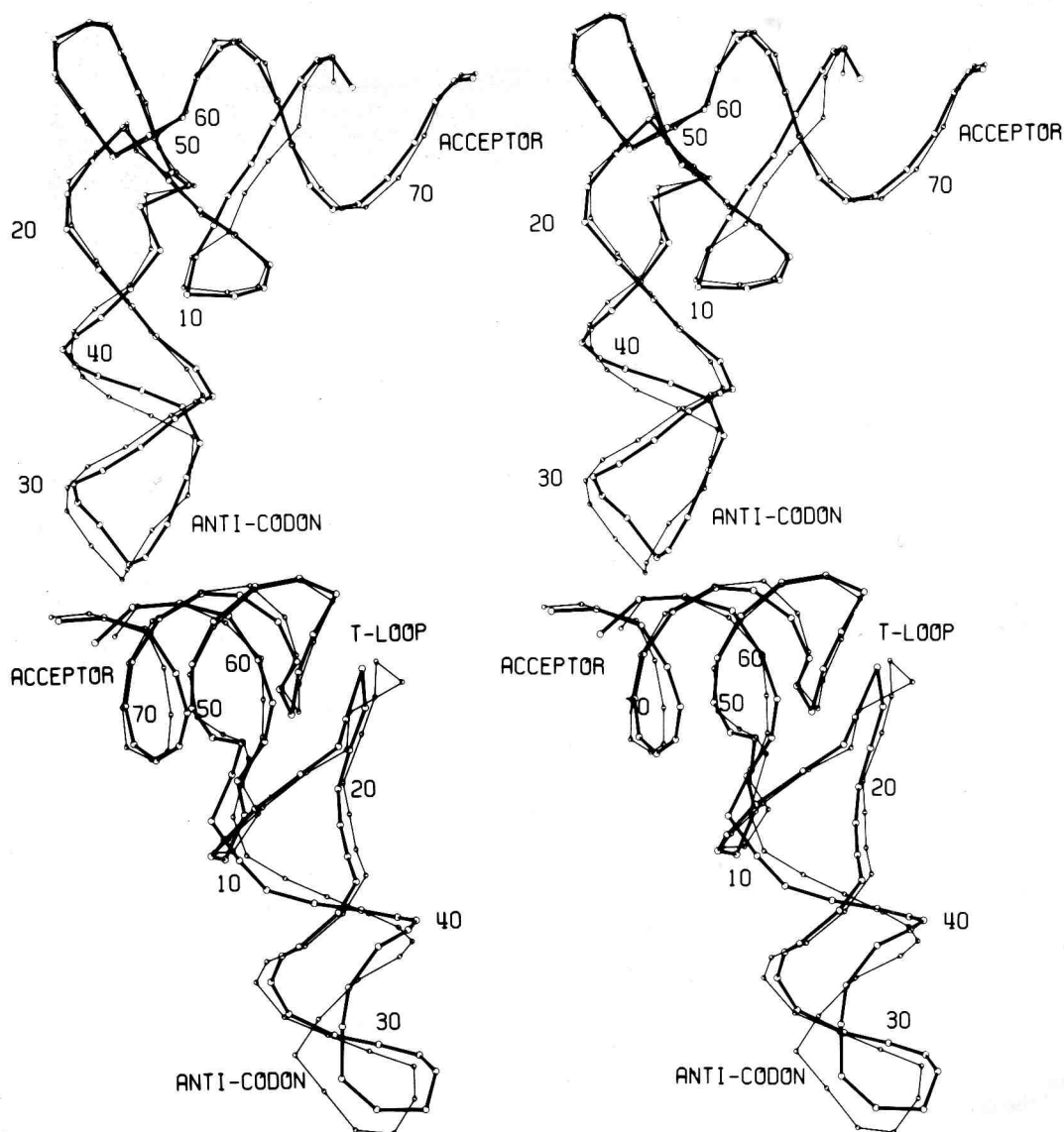


**Fig. 4** Comparison of the yeast tRNA<sup>Met</sup> (heavy line) and yeast tRNA<sup>Phe</sup> (light line) structures in two stereo views. The phosphate backbone is shown with every tenth phosphate residue of yeast tRNA<sup>Met</sup> numbered.

